Zhou *et al. BMC Plant Biology* (2026) 26:1052
https://doi.org/10.1186/s12870-026-08878-z

BMC Plant Biology

RESEARCH Open Access

Multi-omics reveals stage-specific mechanisms of Ginseng response to protopanaxadiol-type ginsenosides stress

Tingting Zhou[1,2], Guiping Wang[1], Xin Li[1], Changbao Chen[1*] and Xin Huang[1*]

Abstract

Background *Panax ginseng* faces continuous cropping obstacles due to autotoxicity from protopanaxadiol-type ginsenosides. Despite studies on individual ginsenosides being reported, the integrated impact of these compounds across different growth stages requires further investigation.

Methods We employed multi-omics approaches to elucidate stage-specific molecular mechanisms in ginseng under protopanaxadiol-type ginsenosides stress. Plants were treated with varying concentrations (10–150 mg/L) of protopanaxadiol-type ginsenosides across four growth stages, followed by integrated transcriptomics, extensively targeted metabolomics, and phytohormone-targeted metabolomics analyses with morphological and physiological assessments.

Results Ginseng plants treated with 100 mg/L protopanaxadiol-type ginsenosides showed stage-specific stress responses. Transcriptomics analysis revealed over 20,000 differentially expressed genes across developmental stages ($P < 0.05$). Significant alterations were observed in pathways related to flavonoids biosynthesis, leading to the identification of 31 key differentially abundant metabolites and 22 critical enzyme genes. Furthermore, 47 differentially expressed genes involved in zeatin biosynthesis and phytohormone signal transduction pathways were identified, potentially regulating the differential accumulation of 8 phytohormones (abscisic acid, jasmonic acid, jasmonoyl-L-isoleucine, salicylic acid, and cytokinins). These molecular responses were putatively associated with enhanced resistance and adaptation to protopanaxadiol-type ginsenosides component stress in ginseng plants. WGCNA identified co-expression modules associated with flavonoid metabolites and phytohormones, providing network-level support for the coordinated regulation between these pathways. Strong correlations were observed between differentially expressed genes and differentially abundant metabolites, suggesting stage-dependent coordinated regulatory networks.

Conclusion Protopanaxadiol-type ginsenosides triggered stage-specific regulatory networks in ginseng, especially during the flowering period stage. Parallel activation of flavonoid biosynthesis and phytohormone signaling pathways contributed to the adaptive response to autotoxicity. These findings provided preliminary insights for

*Correspondence:
Changbao Chen
Fortunate365@163.com
Xin Huang
huangxinrose@163.com

Full list of author information is available at the end of the article

solving continuous cropping obstacle of ginseng and provided a research strategy for investigating stress response mechanisms of plants.

Keywords Ginseng, Protopanaxadiol-type ginsenosides, Autotoxic stress, Multi-omics, Molecular regulatory mechanisms

Background

Medicinal plants are vital strategic resources for global biopharmaceutical innovation, playing an indispensable role in addressing major human health challenges. However, factors such as climate change, ecological degradation, and limitations in cultivation techniques present significant challenges to the quality and yield of medicinal plants. Ginseng (*Panax ginseng* C. A. Meyer) is a traditional East Asian medicinal plant with over 2,000 years of therapeutic history, exemplifying a link between traditional medicine and modern pharmacology [1–3]. Ginseng has a long growth cycle, typically requiring over five years to reach optimal medicinal value, but it faces significant challenges from continuous cropping obstacles. These continuous cropping obstacles resulted from a complex process of ecosystem degradation involving multiple coordination mechanisms, including biotic stress (e.g., pathogen contamination) and abiotic stress (e.g., allelopathic autotoxicity) [4–6]. Among the factors contributing to continuous cropping obstacles, protopanaxadiol-type ginsenosides (PPD) have been identified as critical autotoxins, exerting negative regulatory effects on ginseng plant growth through root exudation and other pathways [7].

Previous studies on the autotoxicity of ginsenosides have revealed several important findings. Ginsenosides R_1, Rg_1, Re, Rg_2, and Rd exhibited autotoxicity to seedling emergence, growth, and root cell viability [8]. Ginsenoside Rb_1 could induce decreased proliferation of ginseng cells and decreased adventitious root branches, thus inhibiting ginseng growth [9]. Ginsenoside Rd showed concentration-dependent autotoxic effects on seed germination and seedling growth of ginseng [10]. Additionally, ginsenosides Rb_1 and Rh_1 showed synergistic effects on promoting pathogen proliferation [11]. Furthermore, ginsenoside Ro stress was found to inhibit ginseng hairy root growth and alter endogenous hormone accumulation [1]. Beyond individual ginsenoside effects, integrated transcriptomics and metabolomics have been applied to investigate ginsenoside autotoxicity during ginseng decomposition [4], and the correlation between ginsenoside polarity and autotoxicity has been explored in hairy root cultures using multi-omics approaches [12].

Despite these advances, critical gaps remain. Previous studies predominantly examined individual ginsenosides rather than ecologically relevant mixtures, relied on in vitro systems (hairy roots or cell cultures) rather than intact plants, and typically employed single or dual omics approaches at single time points. The present study addresses these limitations through four innovations: (1) using PPD-type ginsenoside components at ecologically relevant mass ratios as an integrated stress factor; (2) investigating intact, living P. ginseng plants; (3) integrating three complementary omics layers (transcriptomics, extensively targeted metabolomics, and phytohormone-targeted metabolomics) with morphological and physiological assessments; and (4) systematically comparing molecular responses across four critical developmental stages to identify stage-specific regulatory mechanisms.

In recent years, multi-omics approaches have provided revolutionary breakthroughs in understanding secondary metabolic regulatory mechanisms in plants [13, 14]. This study aimed to investigate the stage-specific molecular mechanisms and regulatory networks of *Panax ginseng* in response to PPD-component stress by integrating transcriptomics, extensively targeted metabolomics, and phytohormone-targeted metabolomics with physiological assessments. The findings provide new insights into ginseng continuous cropping obstacles and offer a research strategy for studying stress response mechanisms in plants.

Materials and methods

Reagents

Malondialdehyde (MDA), superoxide dismutase (SOD), and peroxidase (POD) assay kits (catalog numbers: BC0025, BC0170, and BC0095) were purchased from Beijing Solarbio Science & Technology Co., Ltd. (Beijing, China). Catalase (CAT), soluble protein, soluble sugar, and proline assay kits (catalog numbers: YX-030120P, YX-191618P, YX-191512P, and YX-161815P) were obtained from Shanghai Preferred Biotechnology Co., Ltd. HPLC grade methanol and acetonitrile were procured from Merck & Co., Inc. (Kenilworth, New Jersey, USA), and HPLC grade formic acid was purchased from Aldrich Chemical Company, Inc. (Milwaukee, Wisconsin, USA). 2-chlorophenylalanine (purity: 98%) was purchased from J&K Scientific (Beijing, China).

The protopanaxadiol-type ginsenoside components were prepared using reference standards based on the mass ratios of individual ginsenosides as previously reported by the authors [12]: Rb_1 (1.39 mg/g), Rb_2 (1.29 mg/g), Rc (0.92 mg/g), Rd (0.63 mg/g), Rb_3 (0.39 mg/g), Rg_3 (0.0007 mg/g), and F_2 (0.00006 mg/g). All ginsenosides references were sourced from Chengdu Desite Biotechnology Co., Ltd. (Chengdu, China),

with the following catalog numbers: Rb_1 (DST240702-035), Rb_2 (DSTDR000701), Rc (DSTDR001302), Rd (DSTDR001502), Rb_3 (DSTDR000804), Rg_3 (DSTDR001102), and F_2 (62025-49-4).

Sample preparation

The experiment was conducted in a climate-controlled chamber programmed to simulate natural conditions. Temperature, humidity, and timing parameters were continuously monitored and recorded using an automated touchscreen control system manufactured by Shenzhen Samkoon Technology Co., Ltd. The light environment followed a 12-hour light/12-hour dark cycle, with daytime temperatures maintained at 22℃ (relative humidity: 75%) and nighttime temperatures at 20℃ (relative humidity: 75%). Two-year-old ginseng seedlings, identified as the Fuxing No. 2 variety, were provided by Shenwang Plant Protection Co., Ltd. in Fusong County, Baishan City, Jilin Province. Professor Lianxue Zhang from Jilin Agricultural University authenticated the seedlings as *Panax ginseng* C. A. Meyer of the Araliaceae family.

Three experimental treatments were established:

Blank control group (CK): Healthy forest soil was used as the substrate, with two-year-old ginseng plants. Each treatment consisted of 12 pots, with three *Panax ginseng* plants per pot.

Continuous cropping obstacles group (LSD): Continuous cropping obstacles soil served as the substrate, with other conditions identical to the CK group. The LSD group was included as an ecologically relevant positive control, as continuous cropping soil inherently contains accumulated ginsenosides alongside other co-occurring stress factors (e.g., soil-borne pathogens and deteriorated physicochemical properties), thereby enabling comparison of PPD treatment effects with actual continuous cropping stress conditions.

Protopanaxadiol-type ginsenosides group (PPD): Two-year-old ginseng seedlings were grown in healthy forest soil and treated with protopanaxadiol-type ginsenosides solution via root irrigation on the third day after planting. CK and LSD groups received the same amount of water supplementation. Four different concentrations were applied: 10, 50, 100, and 150 mg/L, with 12 pots per concentration. The gradient was established based on a preliminary systematic survey of PPD-type ginsenoside residues in soils from major ginseng-producing areas in Jilin Province, including Fusong and Ji'an, across different cultivation years (unpublished data). The selected range was designed to encompass the ecologically relevant levels observed in field soils, with 10 mg/L simulating early-stage or mildly affected conditions, 50 and 100 mg/L reflecting levels commonly encountered after multiple years of continuous cropping, and 150 mg/L probing the upper boundary of the dose–response relationship.

Plant samples were harvested at four critical developmental stages: leaf-spreading period (ZYQ, 15 days after germination), flowering period (KHQ, 32 days after germination), fruiting period (JGQ, 105 days after germination), and harvesting period (CSQ, 140 days after germination). To minimize diurnal variation in metabolite content, all samples were collected between 8:00 and 11:00 AM. Immediately after collection, samples were flash-frozen in liquid nitrogen and stored at -80 °C until further analysis.

Detection of physiological resistance indicators

Root morphological indicators were measured at each growth stage. For biochemical analyses, ginseng root samples were homogenized in appropriate extraction solutions. MDA, SOD, POD, CAT, soluble protein (sprotein), soluble sugar, and proline levels were measured using commercial assay kits according to manufacturers' protocols. Biological replicates ($n = 5$) were analyzed per treatment at each growth stage, with data processed using GraphPad Prism (version 10.4).

Detection of ginseng root transcriptomics

Transcriptomic analysis was performed using RNA sequencing (RNA-seq) following standard protocols described in previous studies [4, 12]. Total RNA was extracted from ginseng roots with three biological replicates per treatment at each developmental stage (CK, LSD, and PPD-100 mg/L × four stages = 18 samples in total). Each biological replicate consisted of pooled root tissue from three independent plants. RNA quality was verified by agarose gel electrophoresis, concentration measurement (Qubit 4.0), and integrity evaluation (Qsep400). Libraries were constructed and sequenced on the Illumina platform by Wuhan Maiwei Metabolic Biotechnology Co., Ltd. Differentially expressed genes (DEGs) were identified, with volcano plots generated using Python 3.6.6 and K-means clustering performed in R 4.2.0. KEGG annotation and enrichment analyses were conducted to identify key pathways.

Detection of extensively targeted metabolomics

Freeze-dried and ground ginseng root samples (5 mg) were prepared with three biological replicates per treatment (n = 3) and extracted with 1200 μL precooled 70% methanol containing 2-chlorophenylalanine as an internal standard. After centrifugation and filtration, samples were analyzed using an ExionLC™ AD system with a QTRAP 6500 + mass spectrometer in MRM mode. Mass spectrometry data were analyzed using Analyst 1.6.3

software. Statistical analyses and visualization were performed in R, including PCA, OPLS-DA, and KEGG pathway enrichment of differentially abundant metabolites (DAMs). DAMs were identified using combined criteria of VIP > 1 from OPLS-DA models and fold change ≥ 2 or ≤ 0.5. VIP ≥ 1 indicates above-average contribution to group discrimination [15], and the fold change threshold filters biologically meaningful changes [16]. This dual-filtering strategy minimizes false positives from relying on a single statistical approach [17].

Detection of metabolomics targeted by endogenous phytohormones in plants

50 mg of ground ginseng root samples were prepared with three biological replicates per treatment (n = 3) and used for the extraction of endogenous phytohormones and quantitative analysis using UPLC-MS/MS as described previously [12].

To visualize the overall patterns of phytohormones and their metabolites, clustering heatmaps were generated using the ComplexHeatmap 2.12.0 package in R version 4.2.0. Changes in differentially abundant phytohormones (DAPs) and their metabolites were explored using mirrored bar charts grouped by condition, created with ggplot2 3.4.0 in R version 4.2.2. KEGG enrichment analysis of DAPs and their related metabolites was performed to identify key pathways involved. This analysis was conducted using ggplot2 3.3.0 in R version 4.2.0. Relationships between DAPs and DEGs in key metabolic pathways were analyzed to elucidate the mechanisms driving changes in related biological processes. To visualize these interactions, pathway heatmaps were generated. Correlation plots were created using the corrplot 0.92 package in R version 4.1.2. Validation of key genes identified in the analysis was conducted using qRT-PCR. Reference gene *GAPDH* was selected based on its stable expression.

Correlation analysis and data integration

Pearson correlation analyses were performed to integrate physiological, metabolomic, and transcriptomic data using R software (version 4.3.1). Data were log2-transformed prior to analysis. Statistical significance was assessed with Benjamini-Hochberg correction for multiple testing ($P<0.05$). Correlation heatmaps were generated using the corrplot 0.92 package. Correlations with $|r|>0.5$ and $P<0.05$ were considered biologically meaningful.

Weighted gene co-expression network analysis (WGCNA)

WGCNA was performed using the WGCNA package (v1.72) in R (v4.2.0) with FPKM values from all 18 transcriptome samples [18]. Genes with low expression variation (CV < 0.1) were removed. A soft-thresholding power was selected based on scale-free topology (R^2 > 0.85). Modules were detected using the dynamic tree-cutting algorithm (minimum module size = 30) and merged at eigengene correlation > 0.75. Module–trait relationships were assessed by Pearson correlation between module eigengenes and external traits, including seven key differentially abundant metabolites and eight differentially abundant phytohormones. Intramodular connectivity (kWithin) was used to identify hub genes.

Results

Morphological responses of ginseng to protopanaxadiol-type ginsenoside stress across developmental stages

Varying concentrations of PPD components significantly influenced ginseng growth and development across four key growth stages (ZYQ, KHQ, JGQ, and CSQ) (Supplementary Fig. S1). Visual phenotypic assessment revealed concentration-dependent morphological changes: plants treated with 10 mg/L PPD maintained relatively normal morphology with enhanced green coloration, whereas the 100 mg/L treatment group displayed stunted aerial growth coupled with remarkably proliferated fibrous root systems, creating a distinctive “bushy root” phenotype most prominent during KHQ and JGQ stages. The LSD positive control exhibited similarly extreme morphological changes (Supplementary Fig. S1A).

Comprehensive morphometric analyses (12 biological replicates per treatment, two-way ANOVA with Duncan’s test) confirmed these observations quantitatively (Supplementary Fig. S1B). Among all concentrations tested, the 100 mg/L PPD treatment produced the most pronounced effects: fibrous root number increased approximately 7-fold during KHQ compared to ZYQ (from 5.667 ± 1.528 to 39.667 ± 2.517, $P<0.05$), followed by a significant decline during CSQ. The LSD group exhibited a closely parallel response pattern (from 5.667 ± 1.528 to 37.667 ± 2.082, $P<0.05$), suggesting shared regulatory mechanisms. In the CK group, both fibrous root number and stem height showed significant but comparatively modest changes during KHQ ($P<0.05$), indicating that exogenous PPD amplifies natural developmental transitions. Detailed morphometric data for all concentrations and stages are provided in Supplementary Fig. S1B.

These findings indicated that PPD components exerted stage-specific and concentration-dependent effects on ginseng growth, primarily influencing underground growth characteristics, with a critical threshold at the 100 mg/L concentration that triggered dramatic phenotypic plasticity during KHQ, followed by adaptive adjustments in later developmental stages.

Physiological responses of ginseng plants to protopanaxadiol-type ginsenoside stress

Seven resistance-related physiological indicators (MDA, SOD, POD, CAT, soluble protein, soluble sugar, and proline) were evaluated across all treatment groups and growth stages. All data followed normal distributions (Shapiro-Wilk test) and were analyzed by one-way ANOVA.

The physiological responses displayed a consistent stage-dependent pattern, with the most dramatic changes occurring during KHQ (Fig. 1A–G). MDA content, POD activity, CAT activity, soluble protein, and proline all peaked during KHQ in PPD-treated groups before declining in subsequent stages. Specifically, MDA levels at KHQ in the 10, 50, and 150 mg/L PPD groups were 5.20, 4.58, and 4.78 times higher than in CK, respectively, while POD activity in the 100 mg/L PPD group reached 18.90 times that of CK (Fig. 1A, C). SOD activity displayed a distinct pattern, peaking during ZYQ and subsequently declining, with a partial recovery by CSQ in the 100 mg/L PPD and LSD groups (Fig. 1B). MDA levels in all PPD treatment groups returned to near-normal levels by CSQ, whereas CAT activity remained significantly different from CK across all stages in the 100 mg/L

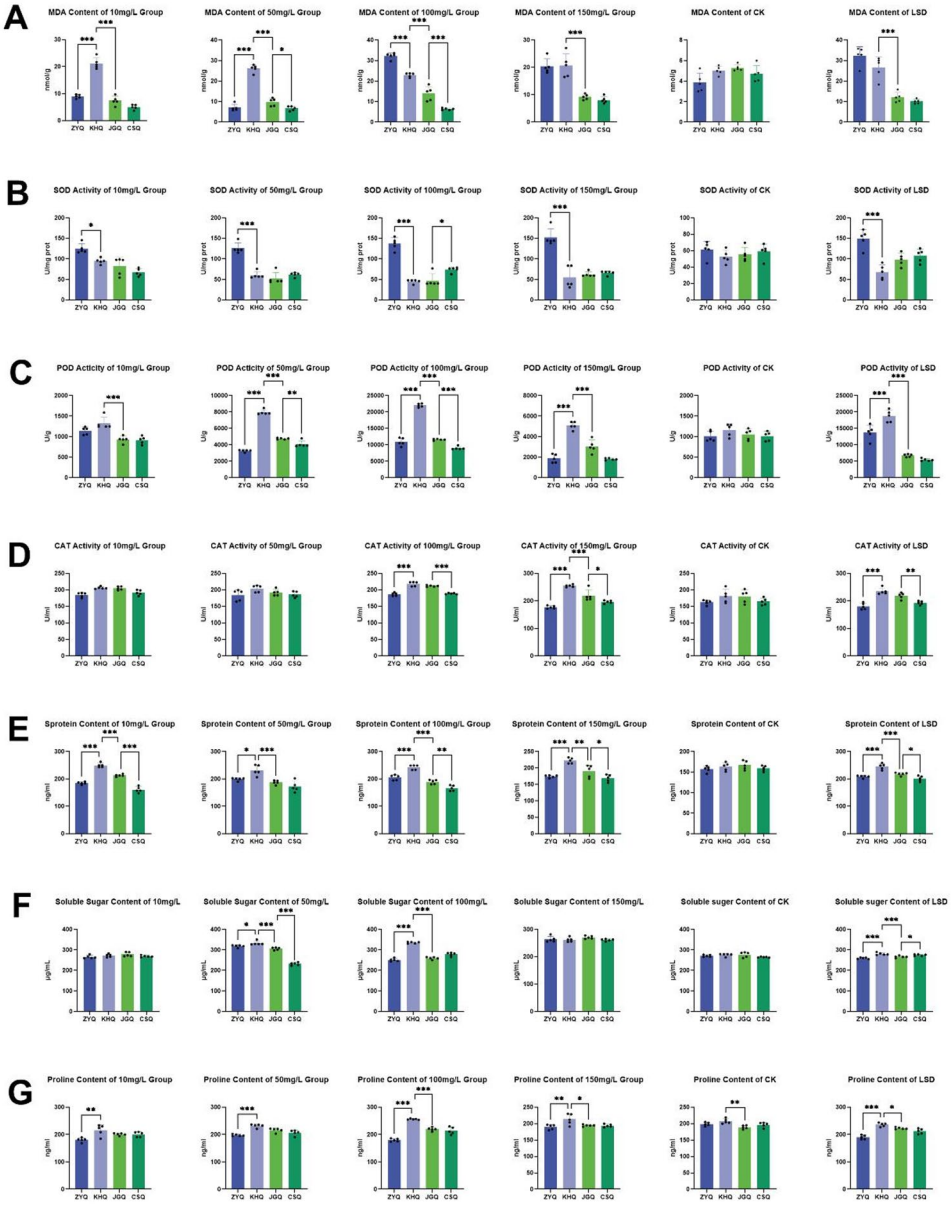

Fig. 1 Changes in resistance physiological indexes of ginseng during different growth stages of different groups: **A** MDA content. **B** SOD activity. **C** POD activity. **D** CAT activity. **E** Sprotein content. **F** Soluble sugar content. **G** Proline content. Ordinary one-way ANOVA analysis was performed for ZYQ vs. KHQ, KHQ vs. JGQ, JGQ vs. CSQ, CSQ vs. CK, and CSQ vs. LSD: $^{*}P < 0.05$, $^{**}P < 0.01$, $^{***}P < 0.001$, $^{****}P < 0.0001$

and 150 mg/L groups ($P < 0.001$), indicating incomplete recovery of this defense mechanism (Fig. 1D). Osmotic regulatory substances (soluble protein, soluble sugar, and proline) similarly peaked during KHQ, with only the LSD group maintaining significant differences from CK at CSQ for protein content (Fig. 1E–G). CK group values remained relatively stable throughout all growth stages for all indicators.

Notably, the 100 mg/L PPD treatment group exhibited significant differences from CK in all seven physiological indicators, with the most pronounced effects during KHQ. Moreover, its response patterns most closely resembled those of the LSD group across multiple indicators (MDA, SOD, POD, fibrous root dynamics), suggesting that this concentration best approximated the autotoxic stress intensity experienced under actual continuous cropping conditions. Consequently, the 100 mg/L PPD stress group, along with CK and LSD groups, were selected for subsequent mechanistic studies. Performing multi-omics analyses across all 4 concentrations and four developmental stages would have been prohibitively costly; selecting the most biologically representative concentration allowed us to focus analytical resources on capturing temporal dynamics, which was the central objective of this study.

Transcriptomic profiling reveals extensive gene expression reprogramming in response to protopanaxadiol-type ginsenoside stress

To investigate the molecular mechanisms underlying the autotoxic effects of PPD components, transcriptome sequencing was performed on ginseng root samples from CK, LSD, and 100 mg/L PPD stress groups in different growth stages (Supplementary Table S1). RNA quality control confirmed that all samples met the requirements for subsequent experiments. After filtering raw data, inspecting sequencing error rates, and analyzing GC content distribution, high-quality clean reads were generated for downstream analyses. The transcriptome data quality was excellent, with Q20 values exceeding 97%, Q30 values surpassing 92%, and GC content ranging between 43% and 44%.

FPKM (Fragments Per Kilobase of transcript per Million fragments mapped) was used to quantify transcript or gene expression levels. DEGs were identified based on the criteria $|\log_2(\text{Fold Change})| \geq 1$ and $\text{FDR} < 0.05$.

Comparisons of KHQ vs. ZYQ, JGQ vs. KHQ, CSQ vs. JGQ, CSQ vs. CK, and CSQ vs. LSD revealed the following: Downregulated genes: 3,361, 15,492, 4,704, 1,481, and 26,976, respectively. Upregulated genes: 6,914, 9,967, 5,484, 2,764, and 17,173, respectively (Supplementary Fig. S2A). Notably, over 20,000 genes exhibited differential expression in JGQ vs. KHQ, with a higher proportion of downregulated genes. The CSQ vs. LSD comparison displayed the largest number of DEGs, totaling 44,149. To further investigate gene expression patterns, all DEGs were subjected to K-means clustering analysis (Supplementary Fig. S2B). These DEGs were grouped into 10 clusters, with Cluster 1 containing 7,563 genes that peaked in expression during KHQ. This pattern was consistent with the accumulation trends of MDA content, POD activity, CAT activity, sprotein content, and proline content described inSect. "Physiological responses of ginseng plants to protopanaxadiol-type ginsenoside stress" Physiological responses of ginseng plants to protopanaxadiol-type ginsenoside stress.

Functional characterization of the DEGs was performed using KEGG annotation and enrichment analyses. DEGs from the comparisons KHQ vs. ZYQ, JGQ vs. KHQ, CSQ vs. JGQ, CSQ vs. CK, and CSQ vs. LSD were enriched in four Level 1 KEGG pathway categories: metabolism, genetic information processing, environmental information processing and organismal systems. Among these, the metabolism category contained the most enriched pathways and genes, while organismal systems had the fewest. The top 20 enriched pathways for each comparison group were displayed in Supplementary Fig. S2C.

The analysis revealed a significant decrease in DEG abundance during ginseng growth from KHQ to JGQ. In contrast, DEG abundance in two enriched pathways increased substantially in CSQ compared to CK, indicating that protopanaxadiol-type ginsenoside components significantly influenced gene expression regulation in ginseng plants. Compared to the CK group, DEGs in CSQ were significantly enriched in pathways related to phenylpropanoid biosynthesis, biosynthesis of secondary metabolites, and biosynthesis of various plant secondary metabolites. These findings suggested that ginseng plants might accumulate secondary metabolites as part of a defense mechanism against stress induced by protopanaxadiol-type ginsenoside components. To further investigate these metabolic responses, a comprehensive targeted metabolomics analysis was performed on ZYQ, KHQ, JGQ, CSQ, CK, and LSD groups.

Additionally, DEGs across all groups were significantly enriched in pathways related to plant endogenous phytohormones, including zeatin biosynthesis, tryptophan metabolism, and plant hormone signal transduction. These results prompted a quantitative analysis of endogenous phytohormone metabolism to further elucidate the molecular mechanisms underlying ginseng's response to protopanaxadiol-type ginsenoside components stress.

Metabolomic analysis reveals significant alterations in flavonoid and phenylpropanoid pathways in response to protopanaxadiol-type ginsenoside stress

A total of 1,830 metabolites were detected, classified into the following categories: amino acids and derivatives (16.67%), phenolic acids (14.1%), terpenoids (11.69%), flavonoids (9.84%), lipids (9.07%), alkaloids (8.52%), lignans and coumarins (5.74%), organic acids (5.68%), nucleotides and derivatives (4.48%), tannins (0.33%), steroids (0.16%), quinones (0.6%), and others (13.11%) (Fig. 2A, Supplementary Table S2).

The PCA score plot (Fig. 2B) demonstrated significant metabolic differences among groups, with minimal variation within samples of the same group. To further refine the analysis, orthogonal partial least squares discriminant analysis (OPLS-DA) was employed. This method incorporated orthogonal signal correction (OSC) and partial least squares discriminant analysis (PLS-DA) to decompose the X matrix (quantitative data for 1,830 metabolites) into Y-related and unrelated information, effectively removing irrelevant variations to identify differential variables. The Y matrix represented the different growth stages of PPD, CK and LSD groups.

The OPLS-DA score plot revealed significant intergroup differences, and the model validation plot indicated excellent predictive power and reliability ($Q^2 = 0.985$, $R^2X = 0.567$, $R^2Y = 0.999$, $P < 0.005$). The robustness of the model was further confirmed by the permutation test, and the S-plot identified a substantial number of significant metabolites with VIP > 1 (Fig. 2C-E).

DAMs were identified among ZYQ, KHQ, JGQ, CSQ, CK, and LSD groups by applying the selection criteria: VIP > 1, fold change ≥ 2 or fold change ≤ 0.5. The total number of DAMs identified in each comparison was as follows: KHQ vs. ZYQ: 520, JGQ vs. KHQ: 404, CSQ vs. JGQ: 254, CSQ vs. CK: 309, CSQ vs. LSD: 347 (Fig. 2F, Supplementary Table S3).

Circular heatmaps were generated to illustrate the relative abundance of these metabolites (Fig. 2G). Interestingly, in the JGQ vs. KHQ comparison, the number of upregulated metabolites was lower than the number of downregulated metabolites, a trend opposite to that observed in the other comparisons. The differential metabolites in each comparison were classified into 13 categories, including amino acids, lipids, terpenoids, flavonoids, and phenolic acids. Ginseng plants showed significant differential accumulation of metabolites under protopanaxadiol-type ginsenoside components stress. These metabolites may be associated with stress resistance and may also act as signaling molecules, triggering specific gene expression and initiating related signal transduction pathways.

Differential metabolites across all comparisons were enriched in three Level 1 KEGG pathway categories: metabolism, genetic information processing and environmental information processing. Further enrichment analysis revealed pathways for KHQ vs. ZYQ, JGQ vs. KHQ,

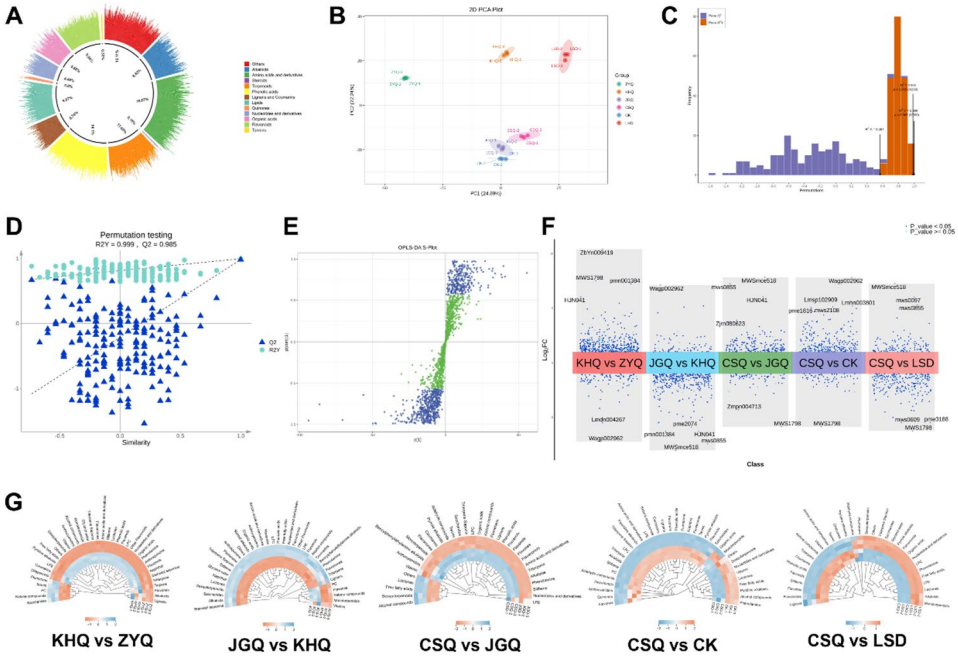

Fig. 2 Establishment of the OPLS-DA model and extensively targeted metabolomics data. **A** PCA score plot. **B** Circle plot for the first-order classification of metabolites. **C** OPLS-DA model validation diagram. **D** OPLS-DA replacement test map. **E** OPLS-DA S-plot. **F** Multi-group differential volcano plot. **G** Ring heat map: Different colors represent the relative magnitude of expression levels

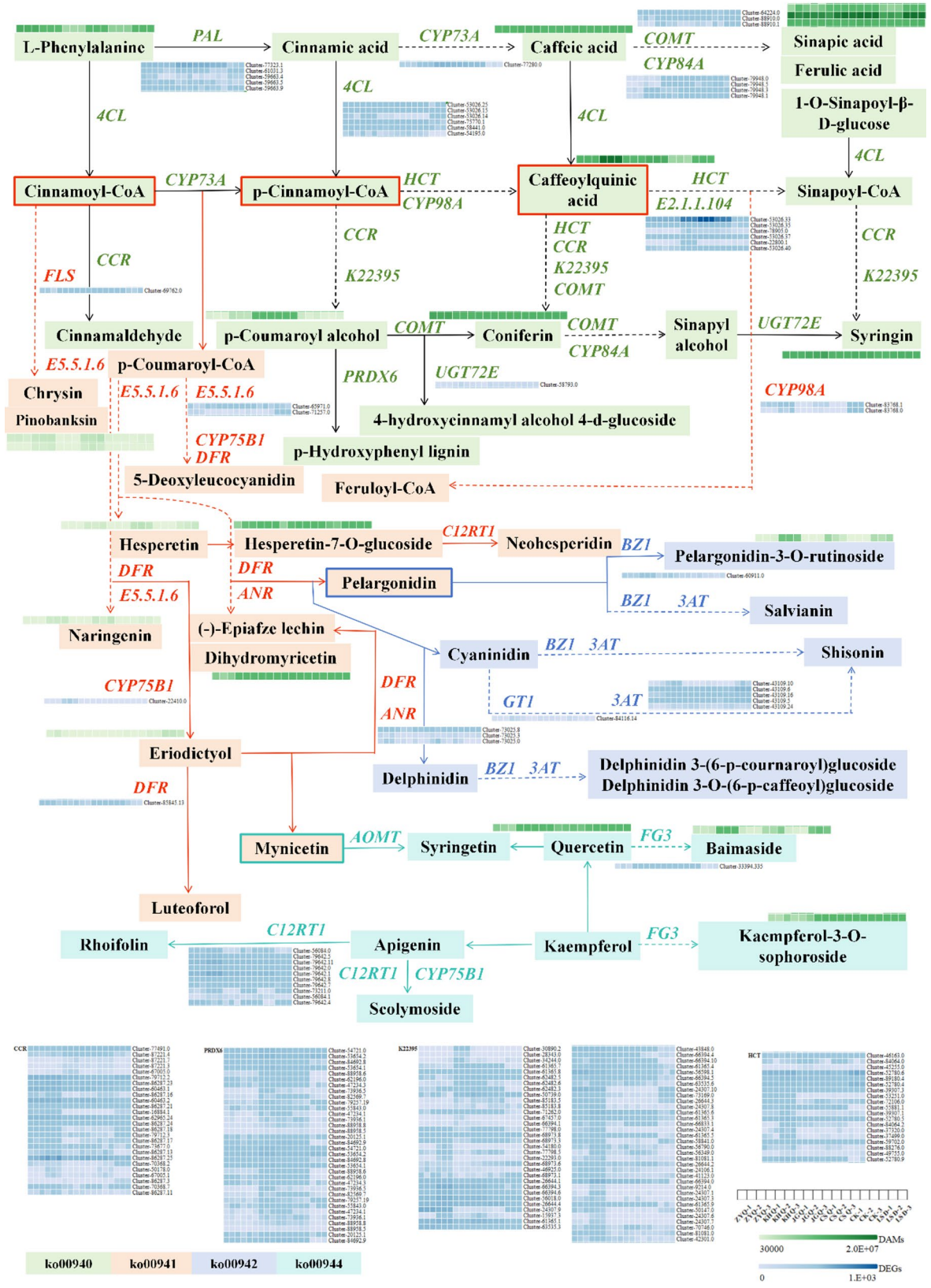

Fig. 3 (See legend on next page.)

(See figure on previous page.)

Fig. 3 Pathway heat map of combined analysis of extensively targeted metabolomics and transcriptomics. Key enzyme gene abbreviations: *PAL*, phenylalanine ammonia-lyase; *4CL*, 4-coumarate-CoA ligase; *CYP73A*, trans-cinnamate 4-monooxygenase; *CMOT*, caffeic acid 3-O-methyltransferase; *CYP84A*, ferulate-5-hydroxylase; *CCR*, cinnamoyl-CoA reductase; *HCT*, shikimate O-hydroxycinnamoyltransferase; *CYP98A*, 5-O-(4-coumaroyl)-D-quinate 3′-monooxygenase; *E2.1.1.104*, caffeoyl-CoA O-methyltransferase; *K22395*, cinnamyl-alcohol dehydrogenase; *PRDX6*, peroxiredoxin 6; *UGT72E*, coniferyl-alcohol glucosyltransferase; *E5.5.1.6*, chalcone isomerase; *FLS*, flavonol synthase; *CYP75B1*, flavonoid 3′-monooxygenase; *DFR*, bifunctional dihydroflavonol 4-reductase; *C12RT1*, flavanone 7-O-glucoside 2″-O-beta-L-rhamnosyltransferase; *ANR*, anthocyanidin reductase; *BZ1*, anthocyanidin 3-O-glucosyltransferase; *3AT*, anthocyanidin 3-O-glucoside 6″-O-acyltransferase; *GT1*, anthocyanidin 5,3-O-glucosyltransferase; *FG3*, flavonol-3-O-glucoside/galactoside glucosyltransferase; *AMOT*, flavonoid O-methyltransferase

CSQ vs. JGQ, CSQ vs. CK, and CSQ vs. LSD were listed in Supplementary Table S4. The top 20 pathways ranked by *P*-value were displayed in Supplementary Fig. S3.

Notably, differential metabolites in CSQ were significantly enriched in pathways such as flavonoid biosynthesis, phenylpropanoid biosynthesis, isoflavonoid biosynthesis, and anthocyanin biosynthesis, highlighting the role of these compounds in stress adaptation. Similar pathways were enriched in the other comparisons, suggesting a potentially important role of flavonoids in ginseng's defense responses.

A combined analysis of metabolomics and transcriptomics revealed common KEGG enrichment pathways, including anthocyanin biosynthesis, phenylpropanoid biosynthesis, flavone and flavonol biosynthesis and flavonoid biosynthesis (Supplementary Fig. S4).

The analysis identified 31 key metabolites, consisting of amino acids and their derivatives, phenolic acids and their derivatives, and various flavonoids. Additionally, 22 key enzymes were identified, including *PAL*, *4CL*, *CYP73A*, *COMT*, *CYP84A*, *HCT*, *CYP98A*, *E2.1.1.104*, *K22395*, *PRDX6*, *UGT72E*, *E5.5.1.6*, *FLS*, *CYP75B1*, *DFR*, *C12RT1*, *ANR*, *BZ1*, *3AT*, *GT1*, *FG3* and *CCR*. Notably, the expression trends of these DEGs were broadly consistent with changes in their putative downstream metabolites. The specific regulatory patterns of key enzymes and key metabolites were described in detail in Fig. 3. A correlation analysis of DEGs and DAMs revealed strong associations between them (Fig. 4A), and qRT-PCR validation further supported the transcriptomic data trends (Fig. 4B).

Among the key metabolites, L-phenylalanine served as the precursor for several phytohormones (e.g., salicylic acid) [19], while caffeic acid and ferulic acid were found to interact with jasmonic acid signaling pathways. These results indicated that protopanaxadiol-type ginsenoside components might induce changes in endogenous phytohormones, which was consistent with the findings from gene expression analysis, where DEGs were enriched in pathways of zeatin biosynthesis and plant hormone signal transduction. Therefore, further analysis of phytohormone metabolism was conducted to identify key response factors and regulatory mechanisms under protopanaxadiol-type ginsenoside components stress.

Protopanaxadiol-type ginsenoside components induce significant changes in phytohormone metabolism and signaling pathways

A total of 44 endogenous phytohormones were identified across all groups (Supplementary Table S5). The PCA revealed that the first principal component explained 38.65% of the dataset's variance, while the second principal component explained 25.58%. Significant differences were observed between groups, with good reproducibility within each group (Supplementary Fig. S5A).

To identify key response factors in ginseng plants under protopanaxadiol-type ginsenoside components stress, differential analyses were conducted on the 44 phytohormones, with fold change ≥ 2 or fold change ≤ 0.5. The results, displayed as mirrored bar charts (Supplementary Fig. S5B-C), revealed significantly differentially accumulated phytohormones.

KEGG pathway enrichment analysis was performed for the DAPs (Supplementary Fig. S5D-H). The significantly enriched pathways primarily included biosynthesis of secondary metabolites, zeatin biosynthesis and plant hormone signal transduction. These findings indicated that protopanaxadiol-type ginsenoside components induced changes in endogenous phytohormone accumulation in ginseng plants, confirming the conclusions of Section.

To validate the co-enriched pathways of DAPs and DEGs, we performed an integrated analysis of targeted phytohormone metabolomics and transcriptomics data. The common KEGG enrichment pathways were obtained (Supplementary Fig. S6), including plant hormone signal transduction and zeatin biosynthesis.

Key DAPs and their related metabolites were identified as DHZR, cZR, tZR, IPR, JA-ILE, JA, ABA, and SA. Furthermore, a total of 47 key enzymes were identified, including: *TRIT1*, *IPT*, *CYP735A*, *UGT85A*, *CKX*, *UGT76C1_2*, *AUX1*, *TIR1*, *IAA*, *ARF*, *GH3*, *SAUR*, *AHK2_3_4*, *AHP*, *ARR-B*, *ARR-A*, *GID1*, *DELLA*, *PIF3*, *PYL*, *PP2C*, *SNRK2*, *ABF*, *CTR1*, *ETR*, *MKK4_5*, *MPK6*, *EIN2*, *EBF1_2*, *EIN3*, *ERF1*, *BAK1*, *BKI1*, *BRI1*, *BSK*, *TCH4*, *CYCD3*, *BIN2*, *BZR1_2*, *JAR1_4_6*, *COI-1*, *JAZ*, *MYC2*, *NPR1*, *TGA*, and *PR1*. Pathways heatmap was constructed to visualize the co-regulatory networks of key phytohormones and genes (Fig. 5).

In the zeatin biosynthesis pathway, *UGT85A* was associated with the highest number of genes. Additionally, two *IPT* genes, four *CKX* genes, and two *TRIT1* genes

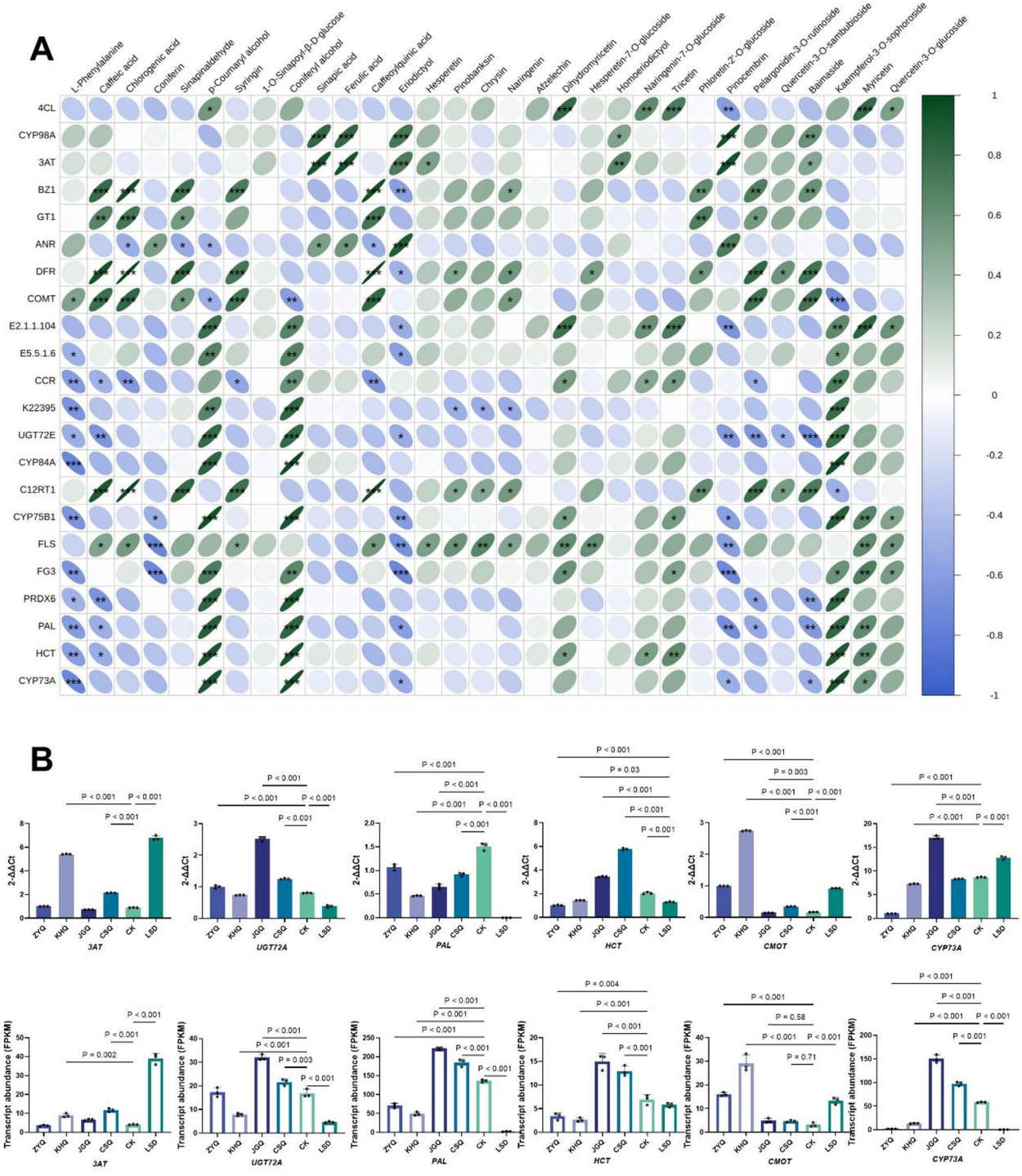

Fig. 4 Relationship between DAMs and DEGs. **A** Correlation corplot of key DAMs and key DEGs. **B** qPCR verification results and DEGs' transcript abundance (FPKM, fragments per kilobase of transcript per million mapped reads)

showed peak expression during KHQ. Comparatively, the plant hormone signal transduction pathway exhibited broader regulatory changes, with over 600 genes affected. Genes such as *ARF*, *ARR-B*, *DELLA*, *PP2C*, *BAK1*, *BRI1*, *BSK*, *JAZ*, and *MYC2* exhibited dozens or even hundreds of differentially expressed members. Notably, Cluster-70614.1 of *PYL* exhibited the highest expression, particularly during CSQ. The accumulation trend of JA-ILE closely corresponded to the expression trends of six *JAR1_4_6* genes. Three *JAZ* genes, five *TCH4* genes, and one *GID1* gene were significantly upregulated in ZYQ and KHQ, while two *PR1* genes exhibited high expression

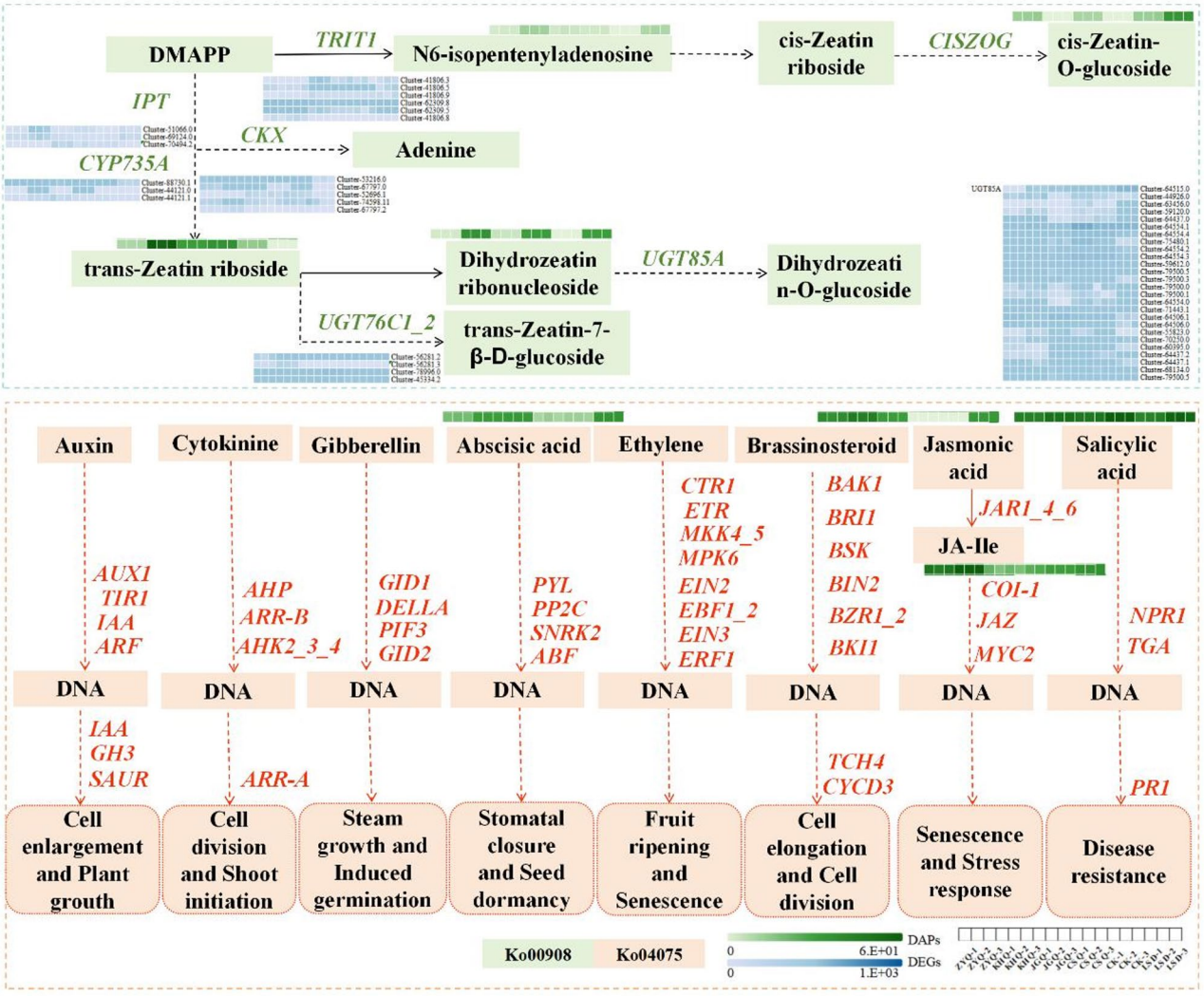

Fig. 5 Pathway heat map of the combined analysis of phytohormone-targeted metabolomics and transcriptomics. Key enzyme gene abbreviations: *TRIT1*, tRNA dimethylallyltransferase; *IPT*, adenylate dimethylallyltransferase (cytokinin synthase); *CYP735A*, cytokinin trans-hydroxylase; *UGT85A*, UDP-glucosyltransferase 85A; *CKX*, cytokinin dehydrogenase; *UGT76C1_2*, cytokinin-N-glucosyltransferase; *AUX1*, auxin influx carrier; *TIR1*, transport inhibitor response 1; *IAA*, auxin-responsive protein IAA; *ARF*, auxin response factor; *GH3*, auxin responsive GH3 gene family; *SAUR*, SAUR family protein; *AHK2_3_4*, arabidopsis histidine kinase 2/3/4; *AHP*, histidine-containing phosphotransfer peotein; *ARR-A*, two-component response regulator ARR-A family; *ARR-B*, two-component response regulator ARR-B family; *GID1*, gibberellin receptor GID1; *DELLA*, DELLA protein; *PIF3*, phytochrome-interacting factor 3; *GID2*, F-box protein GID2; *PYL*, abscisic acid receptor PYR/PYL family; *PP2C*, protein phosphatase 2C; *SNRK2*, serine/threonine-protein kinase SRK2; *ABF*, ABA responsive element binding factor; *CTR1*, rine/threonine-protein kinase CTR1; *ETR*, ethylene receptor; *MKK4_5*, mitogen-activated protein kinase kinase 4/5; *MPK6*, mitogen-activated protein kinase 6; *EIN2*, ethylene-insensitive protein 2; *EBF1_2*, EIN3-binding F-box protein; *EIN3*, ethylene-insensitive protein 3; *ERF1*, thylene-responsive transcription factor 1; *BAK1*, brassinosteroid insensitive 1-associated receptor kinase 1; *BKI1*, BRI1 kinase inhibitor 1; *BRI1*, protein brassinosteroid insensitive 1; *BSK*, BR-signaling kinase; *TCH4*, xyloglucan: xyloglucosyl transferase TCH4; *CYCD3*, cyclin D3; *BIN2*, shaggy-related protein kinase (protein brassinosteroid insensitive 2); *BZR1_2*, brassinosteroid resistant 1/2; *JAR1_4_6*, jasmonic acid-amino synthetase; COI-1, coronatine-insensitive protein 1; *JA*, jasmonate ZIM domain-containing protein; *MYC2*, transcription factor MYC2; *NPR1*, regulatory protein NPR1; *TGA*, transcription factor TGA; *PR1*, pathogenesis-related protein 1

in KHQ. Additionally, two *PYL* genes showed significantly elevated expression in CSQ and LSD. The heat map illustrated the changes in key DEGs of the Ko04075 pathway (Supplementary Fig. S7).

The correlation analysis revealed that the key DAPs showed strong correlations with the key DEGs (Fig. 6A). qRT-PCR validation of randomly selected genes confirmed that their relative expression levels were consistent with transcriptome data trends (Fig. 6B).

Integration of physiological responses with molecular mechanisms

To investigate the intrinsic connections between physiological adaptations and molecular changes, we performed

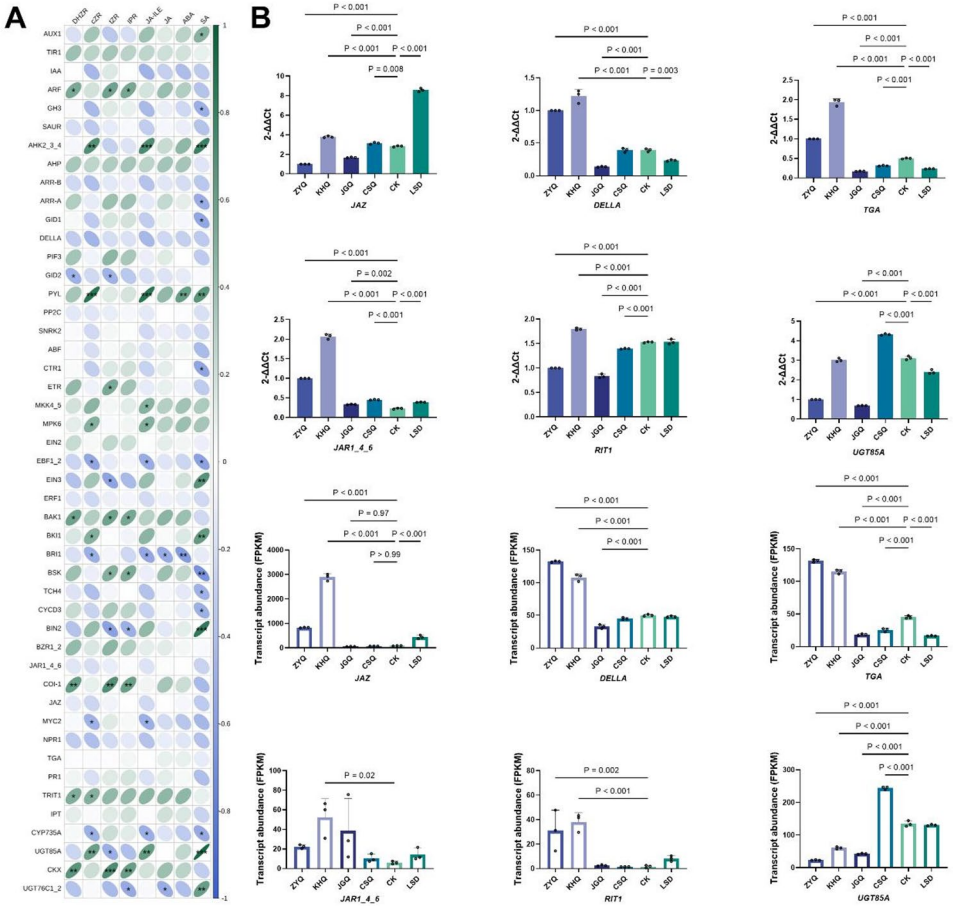

Fig. 6 Relationship between DAPs and DEGs. **A** Correlation corplot of key DAPs and key DEGs. **B** qPCR verification results and DEGs' FPKM

comprehensive correlation analyses integrating resistance physiological indices with metabolomic and transcriptomic data across all treatment groups (100 mg/L PPD at ZYQ, KHQ, JGQ, CSQ stages, plus CK and LSD at CSQ stage).

Correlations between physiological indices and flavonoid metabolism

Correlation analysis revealed strong associations between physiological stress indicators and flavonoid metabolic reprogramming at both metabolite and gene expression levels (Supplementary Fig. S8A-B).

At the metabolite level, oxidative stress marker MDA showed strong positive correlations with phenylpropanoid pathway intermediates, including L-phenylalanine ($P<0.05$) and coniferin ($P<0.01$). Antioxidant enzymes (POD and CAT) and osmotic adjustment indicators (sprotein, soluble sugar, proline) exhibited similar positive correlation patterns with caffeic acid ($P<0.05$), chlorogenic acid ($P<0.01$), as well as lignin precursors such as sinapinaldehyde ($P<0.05$). Notably, several flavonoid aglycones (kaempferol-3-O-sophoroside, quercetin-3-O-glucoside) showed either weak or negative correlations with stress indicators, suggesting their conversion to glycosylated forms under stress.

At the transcriptional level, these metabolic patterns were supported by corresponding gene expression correlations. Core phenylpropanoid pathway genes showed strong responses: *DFR* exhibited strong positive correlations with oxidative stress markers ($P<0.01$). Flavonoid glycosylation genes demonstrated distinct patterns: *BZ1* showed positive correlations with most stress parameters ($P<0.05$), while *GT1* displayed mixed correlation patterns. Methylation enzyme *COMT* showed strong positive correlations with most physiological indices ($P<0.05$), supporting enhanced lignification under stress. Interestingly, some biosynthetic genes like *CCR* exhibited negative correlations with certain stress markers, suggesting complex metabolic flux regulation within the phenylpropanoid-flavonoid network.

Correlations between physiological indices and phytohormone signaling

Correlation analyses revealed coordinated relationships between hormone signaling and physiological responses

at both metabolite and transcriptional levels (Supplementary Fig. S8C-D).

At the hormone level, ABA and JA showed positive correlations with CAT activity and proline accumulation ($P < 0.05$), confirming stress hormone activation. Cytokinins (DHZR, cZR, tZR, IPR) consistently correlated with POD, CAT, and proline content, suggesting their role in stress mitigation. Conversely, SA showed negative correlations with MDA and POD ($P < 0.05$).

At the transcriptional level, these patterns were reinforced by corresponding gene expression. ABA signaling components (*ABF*, *PP2C*, *SNRK2*) and downstream targets (*GID1*, *DELLA*) showed strong positive correlations with most stress indicators ($P < 0.05$). JA pathway genes (*JAR1_4_6*) and ethylene signaling components (*ERF1*, *CTR1*) similarly exhibited positive correlations with physiological parameters ($P < 0.05$). Auxin signaling displayed complex regulation, with response factors (*ARF*, *SAUR*) positively correlating while receptors (*TIR1*, *AUX1*) negatively correlating with most stress indices. Brassinosteroid signaling showed mixed responses, with BSK and TCH4 positively but BRI1 and BKI1 negatively correlating with stress markers ($P < 0.05$).

These integrated hormone-physiology correlations suggested that PPD autotoxicity coordinated a multi-layered hormonal response network, with ABA and JA putatively driving stress adaptation while other hormones potentially modulating specific aspects of the defense response.

WGCNA identified gene modules associated with flavonoid metabolism and phytohormone traits

WGCNA yielded 19 co-expression modules (125–9,177 genes). Module–trait correlation analysis identified five modules with simultaneous significant correlations with both metabolite and phytohormone traits (Supplementary Fig. S9; Supplementary Table S6).

The blue and brown modules displayed reciprocal correlation patterns. The blue module was positively correlated with phenylpropanoid intermediates but negatively correlated with kaempferol-3-O-sophoroside and SA, whereas the brown module showed the opposite pattern. This was consistent with a transition from upstream intermediate accumulation to downstream flavonol production. The lightcyan module was positively correlated with both flavonol glycosides and cytokinins while negatively correlated with SA. The greenyellow module was strongly associated with phenylpropanoid intermediates.

The grey60 module (207 genes) showed strong concurrent correlations with multiple phytohormones (cZR, JA-ILE, and ABA; all $P < 0.001$). The top hub gene was a 60 S ribosomal protein L8 (Cluster-77051.3, kWithin = 80.25). This module contained cinnamyl-alcohol dehydrogenase (*K22395*) and flavanone 7-O-glucoside 2″-O-beta-L-rhamnosyltransferase (*C12RT1*), both of which were identified as DEGs in the phenylpropanoid and flavonoid biosynthesis pathways (Sect. "Protopanaxadiol-type ginsenoside components induce significant changes in phytohormone metabolism and signaling pathways"), as well as JA biosynthesis-related genes, antioxidant genes (Cu-Zn SOD, glutathione S-transferase), and three transcription factors (*WRKY22*, *HOX11*, *ZAT11*). The co-expression of these functionally diverse genes within a single module suggested potential co-regulation between secondary metabolism and hormone signaling pathways.

Discussion

This study investigated the molecular mechanisms by which protopanaxadiol (PPD)-type ginsenoside components influenced *Panax ginseng* growth across four developmental stages (ZYQ, KHQ, JGQ, and CSQ), integrating phenotypic, physiological, transcriptomic, metabolomic, and phytohormone analyses.

Concentration- and stage-dependent effects on ginseng growth

The effects of PPD-type ginsenosides on ginseng growth were concentration- and stage-dependent. Low-concentration treatment (10 mg/L) induced a redistribution of growth resources that favored aboveground development over root expansion, reflecting an adaptive response to mild stress. Medium-concentration treatments (50 and 100 mg/L) caused significant fluctuations in fibrous root numbers, while main root growth remained relatively stable, indicating that ginsenoside stress primarily impacted the fibrous root system. This finding may provide new insight into root system decline associated with ginseng continuous cropping obstacles. High-concentration treatment (150 mg/L) produced more pronounced fluctuations in fibrous root development and increased stem height, with the most significant effects observed during the active growth stages (KHQ–JGQ). The response pattern of the LSD group was consistent with that of the 100 mg/L treatment group.

However, it should be noted that the LSD group inherently encompassed multiple co-occurring stress factors beyond ginsenosides, including soil-borne pathogens and deteriorated physicochemical properties, and the PPD-type ginsenoside concentration in the LSD soil was not quantified in this study. Therefore, the phenotypic and molecular similarities observed between the two groups should be interpreted as evidence supporting the prominent role of PPD-type ginsenosides in continuous cropping obstacles, rather than implying equivalent stress conditions. The divergence between them likely reflected the additive or synergistic effects of other stress components present in the LSD soil. Future studies incorporating quantitative analysis of ginsenoside residues in continuous cropping soil would further clarify the

relative contribution of PPD-type ginsenosides to the overall continuous cropping obstacle effect.

Activation of multiple physiological defense systems

Plants activated multiple defense systems when exposed to abiotic stress. This study observed three primary defensive responses of ginseng plants under protopanaxadiol-type ginsenoside components stress.

Firstly, the membrane system protection mechanisms were activated. MDA is a major product of lipid peroxidation in membranes, and its accumulation damages cell membranes and organelles [12, 20]. The increase in MDA levels indicated an increased degree of lipid oxidation and more severe cellular damage [21]. In the 100 mg/L protopanaxadiol-type ginsenoside treatment group, MDA content peaked during the ZYQ stage, while in the other three treatment groups, the highest accumulation occurred during the KHQ stage. In contrast, the CK group maintained relatively stable MDA levels throughout all growth stages. This suggested that the 100 mg/L treatment triggered an earlier stress response.

Secondly, the antioxidant enzyme system was coordinately activated. The antioxidant enzyme system plays a crucial role in mitigating oxidative stress induced by ginsenoside components. SOD as the first line of defense [22], exhibited peak activity during the ZYQ stage across all treatment groups, indicating its rapid scavenging of reactive oxygen species (ROS). POD acted as a double-edged sword, while it alleviates peroxide-induced membrane damage and protects the plant, it can also contribute to ROS production, chlorophyll degradation, and membrane lipid peroxidation, potentially causing damage [23, 24]. CAT activity in the high-concentration groups (100 and 150 mg/L) significantly increased during the KHQ stage ($P < 0.001$), reflecting elevated H_2O_2 levels [25, 26]. Together, these enzymes appeared to form a comprehensive ROS scavenging network: SOD responded rapidly during ZYQ, POD activity rose significantly during KHQ, and CAT showed sustained enhancement under high concentrations.

Thirdly, targeted accumulation of osmoregulatory substances. Osmoregulatory substances (soluble sugars, proline, and soluble proteins) in all treatment groups followed a consistent pattern of initial increase followed by decrease, highlighting their role in maintaining cellular osmotic balance and stabilizing enzyme activity under stress [27, 28].

Dynamic reprogramming of flavonoid metabolic networks

Flavonoids are essential secondary metabolites regulated by a complex biosynthetic network involving phenylpropanoid, flavonoid, anthocyanin, and flavonol biosynthesis pathways [29]. This study explored the molecular responses and functional reprogramming of these pathways under PPD-type ginsenoside stress.

Anthocyanins, highly active glycosylated polyphenolic compounds, play a key role in plant stress responses [30, 31]. These compounds not only exhibit strong antioxidant activities, but also significantly enhance plant tolerance to abiotic stress [32, 33]. As a critical branch of the flavonoid biosynthesis pathway, anthocyanin biosynthesis involves a sequence of complex enzyme-catalyzed reactions. In this study, the differential expression of anthocyanidin 3-O-glucosyltransferase, *BZ1* was associated with the accumulation of pelargonidin-3-O-rutinoside, which peaked during the KHQ stage. This finding suggested that plants may have regulated gene expression and adjusted metabolic pathways to establish defense responses during the early stages of stress.

In the phenylpropanoid pathway, key enzymes including phenylalanine ammonia-lyase (*PAL*), cinnamate-4-hydroxylase (*C4H*), and 4-coumarate-CoA ligase (*4CL*) catalyzed the formation of p-coumaroyl-CoA, an essential precursor for downstream branches [34–36]. Notably, cinnamoyl-CoA reductase (CCR) may regulate flavonoid biosynthesis through substrate competition with the lignin pathway [37]. Six key phenolic acid compounds accumulated under stress, contributing antioxidant, free radical scavenging, and antimicrobial activities that enabled ginseng plants to resist PPD-type ginsenoside-induced stress [38, 39].

Flavonoids are crucial secondary metabolites that play an essential role in plant defenses against biotic and abiotic stress. Their complex biosynthetic mechanisms represent a frontier in plant science research [40–42]. In the flavonoid biosynthesis pathway, ten key genes and eleven metabolites were identified. Flavonol synthase (*FLS*) regulated the accumulation of chrysin and pinobanksin while competing with dihydroflavonol-4-reductase (*DFR*) for the same substrate, reflecting fine metabolic balance [43–45]. *CYP75B1*, a cytochrome *P450* protein, showed steadily increasing expression from ZYQ to CSQ, catalyzing the production of eriodictyol and thereby enhancing antioxidant defenses [46].

In the flavone and flavonol pathway, three flavonol compounds and three key regulatory genes were identified. FG3 regulated the accumulation of kaempferol-3-O-sophoroside, a flavonol glycoside with strong free radical scavenging activity [47, 48], further confirming that ginseng plants constructed multiple defense systems through metabolic reprogramming.

Dynamic reprogramming of phytohormone signaling

Cytokinins exhibited significant dynamic changes under PPD-type ginsenoside stress [49, 50]. By precise quantitative analysis, significant dynamic changes in the key cytokinin transport forms, cis-Zeatin (cZR) and trans-Zeatin

(tZR) ribosides, across growth stages were presented [51]. During the late KHQ stage, concentrations of dihydrozeatin riboside (DHZR), tZR, and isopentenyl riboside (IPR) peaked at 11.7 ng/g, 54.9 ng/g, and 1.4 ng/g, respectively. These findings suggested that plants constructed molecular defense mechanisms against stress by coordinating the accumulation of tZR and DHZR through *IPT* and *CYP735A* enzyme pathways, and regulating IPR metabolism via the *TRIT1* gene [52, 53]. These coordinated metabolic changes suggested the critical role of cytokinin reprogramming in stress adaptation.

Multiple phytohormone signaling pathways were dynamically regulated under stress [54]. Salicylic acid (SA) increased continuously from ZYQ to a peak of 93.9 ng/g during CSQ (3.5 times higher than CK), suggesting activation of the systemic acquired resistance (SAR) mechanism [55, 56]. Jasmonic acid (JA) peaked during JGQ but declined significantly during CSQ, indicating stage-specific regulation particularly involving root growth and reproductive development. Abscisic acid (ABA) peaked at 8.4 ng/g during JGQ (six times higher than CK), suggesting that defense mechanisms were initiated through stomatal closure. The activation of the negative regulator PP2C further modulated ABA signal transduction and stabilized ABA levels during the CSQ stage.

Beyond these individual hormone dynamics, the temporal profiles observed in our study provided suggestive evidence for three hormone cross-talk mechanisms potentially operating during ginseng's response to PPD-type ginsenoside stress. First, ABA and JA exhibited concurrent accumulation during the JGQ stage, accompanied by significant positive correlations with CAT activity and proline content ($P < 0.05$), and the coordinated upregulation of SnRK2, ABF, and JAR1_4_6. This pattern was consistent with the previously reported ABA–JA synergy mediated through the MYC2 transcription factor, a shared signaling node known to integrate both ABA- and JA-dependent defense responses [57, 58]. The concurrent activation of *SnRK2* and *JAR1_4_6* may have reflected a putative *MYC2*-mediated convergence of these two pathways, although direct validation in ginseng remained to be conducted. Second, SA and JA displayed an inverse temporal pattern: SA accumulated continuously toward CSQ while JA declined after peaking at JGQ. This reciprocal dynamic was reminiscent of the well-characterized SA–JA antagonism, in which *NPR1* suppressed JA-responsive gene expression downstream of the *SCF COI1-JAZ* complex [59, 60]. The progressive SA accumulation observed in our study may have gradually attenuated JA signaling, implying a possible shift from JA-mediated defense toward SA-mediated systemic acquired resistance. Third, cytokinins peaked during KHQ whereas ABA peaked later during JGQ, suggesting a temporal transition from growth-promoting to stress-adaptive regulation. This sequential pattern was in line with the antagonistic relationship between cytokinin and ABA signaling, in which type-B ARRs physically interacted with *SnRK2s* and repressed their kinase activity in *Arabidopsis* [61], although whether an analogous mechanism operated in *Panax ginseng* required further investigation. Collectively, while definitive mechanistic conclusions awaited further functional validation, our integrated data suggested that ginseng plants may have orchestrated a temporally coordinated hormonal network, with the KHQ–JGQ transition representing a putative inflection point from growth promotion to stress defense.

Integration of multi-level responses

Correlation analyses provided crucial evidence linking physiological adaptations with molecular reprogramming. The strong positive correlations between MDA and phenylpropanoid intermediates (L-phenylalanine, $P < 0.05$; coniferin, $P < 0.01$) suggested that oxidative stress may have contributed to secondary metabolic responses. This was further supported by the coordinated upregulation of biosynthesis genes, with DFR showing strong positive correlations with oxidative stress markers ($P < 0.01$), and *BZ1*, *COMT* exhibiting significant correlations with most stress parameters ($P < 0.05$).

The positive correlations between stress hormones (ABA, JA) and CAT activity as well as proline accumulation ($P < 0.05$), along with their corresponding signaling genes (*ABF*, *PP2C*, *SNRK2* for ABA pathway; *JAR1_4_6* for JA pathway), demonstrated functional links between hormonal regulation and physiological stress responses. Notably, cytokinins (*DHZR*, *cZR*, *tZR*, *IPR)* consistently correlated with POD, CAT, and proline content, suggesting their role in stress mitigation beyond growth regulation. Interestingly, SA showed negative correlations with MDA and POD ($P < 0.05$), indicating distinct regulatory patterns among different hormones.

These integrated analyses revealed that the physiological, metabolic, and transcriptional changes formed a coordinated defense network rather than operating in isolation. The complex correlation patterns, including both positive and negative associations, reflected sophisticated metabolic flux regulation within the defense network. However, further time-course experiments with pathway-specific inhibitors would help establish causal relationships and distinguish between parallel independent responses and interconnected regulatory cascades. WGCNA provided network-level support for the coordinated relationship between flavonoid metabolism and phytohormone signaling observed in previous sections. The reciprocal patterns of the blue and brown modules were consistent with the metabolic flux transition from

phenylpropanoid intermediates to flavonol end-products discussed in Sect. "Dynamic reprogramming of flavonoid metabolic networks". The co-occurrence of *K22395* and *C12RT1*, previously identified as DEGs in phenylpropanoid and flavonoid pathways (Sect. "Protopanaxadiol-type ginsenoside components induce significant changes in phytohormone metabolism and signaling pathways"), within the grey60 module alongside JA biosynthesis-related genes and stress-responsive transcription factors (*WRKY22*, *HOX11*, *ZAT11*) suggested that these pathways may be co-regulated at the transcriptional level. However, the predominance of ribosomal proteins among hub genes in this module indicated that translational regulation may also be involved in coordinating these responses, a possibility that warrants further investigation. Functional validation through genetic approaches would be required to establish causal relationships among the identified hub genes.

Novelty and limitations

Collectively, the present study advanced beyond previous ginsenoside autotoxicity research, which, despite progress in characterizing the effects of individual ginsenosides and ginsenoside fractions or decomposition productshas largely relied on in vitro systems and single-stage experimental designs. By applying ecologically relevant PPD-type ginsenoside mixtures to intact ginseng plants and integrating transcriptomic, metabolomic, and phytohormone analyses across four developmental stages, this work provided several novel biological insights that were unlikely to be captured by conventional approaches. Specifically, we identified KHQ as a critical developmental window in which oxidative damage, antioxidant enzyme activation, and flavonoid metabolic reprogramming converged most intensely, and suggested that the coordination between flavonoid biosynthesis and phytohormone signaling pathways was stage-dependent rather than constitutive. These findings provided a new temporal dimension for understanding ginsenoside-mediated autotoxicity and offered potential targets for mitigating continuous cropping obstacles in *Panax ginseng* cultivation.

It should be noted that transcriptome sequencing for the CK and LSD groups was only performed at the harvest stage (CSQ), rather than across all developmental stages. This design prioritized capturing the temporal dynamics of molecular responses within the PPD treatment group and assessing the cumulative effects at the agronomically relevant endpoint. Although the physiological indices measured across all groups and stages confirmed that CK exhibited minimal variation throughout the growth cycle, supporting the interpretation of within-PPD temporal comparisons as primarily reflecting stress responses, full temporal transcriptome profiling of control groups would enable more precise separation of developmental and stress-induced gene expression changes. Future studies incorporating such comprehensive designs are warranted.

Conclusions

This study investigated the mechanisms of *Panax ginseng* autotoxicity mediated by protopanaxadiol-type ginsenoside components using multi-omics integration. The key findings were summarized as follows. The effects of protopanaxadiol-type ginsenoside components on *Panax ginseng* growth and development exhibited significant concentration dependency and stage specificity, primarily manifested as root growth inhibition and marked changes in physiological resistance indicators. The protopanaxadiol-type ginsenoside components significantly altered the accumulation patterns of flavonoid and phenolic acid compounds by regulating secondary metabolic pathways, and predominantly regulated the gene expression of key pathways, including those involved in secondary metabolite biosynthesis and phytohormone signal transduction. Endogenous phytohormone analysis revealed significant changes in the levels of key phytohormones, including cZR, ICAld, tZR, and tZRMP. Furthermore, the temporal hormone profiles provided suggestive evidence for coordinated cross-talk among ABA–JA, SA–JA, and cytokinin–ABA signaling axes, with the KHQ–JGQ transition representing a putative inflection point from growth promotion to stress defense, although the precise molecular mechanisms underlying these interactions in *Panax ginseng* remain to be functionally validated.

Based on these findings, a preliminary growth regulation network induced by protopanaxadiol-type ginsenosides was proposed, which may provide a useful theoretical reference for further understanding the mechanism of *Panax ginseng* autotoxicity and addressing the problem of *Panax ginseng* continuous cropping obstacles. From a practical perspective, the results may inform strategies for optimizing planting practices, such as adjusting planting density and ginsenoside residue management, to mitigate autotoxic effects. Additionally, the study offered foundational insights for the development of *Panax ginseng* varieties with enhanced tolerance to continuous cropping stress, which could potentially improve yield and sustainability in *Panax ginseng* agriculture.

Abbreviations

PPD	Protopanaxadiol-type ginsenosides
ZYQ	Leaf-spreading period
KHQ	Flowering period
JGQ	Fruiting period
CSQ	Harvesting period
CK	Blank control group
LSD	Continuous cropping obstacles Group
MDA	Malondialdehyde

SOD	Superoxide dismutase
POD	Peroxidase
CAT	Catalase
Sprotein	Soluble protein
DEGs	Differentially expressed genes
DAMs	Differentially abundant metabolites
DAPs	Differentially abundant phytohormones
FPKM	Fragments Per Kilobase of transcript per Million fragments mapped
OPLS-DA	Orthogonal partial least squares discriminant analysis
OSC	Orthogonal signal correction
PLS-DA	Partial least squares discriminant analysis
PCA	Principal component analysis
PAL	Phenylalanine ammonia-lyase
4CL	4-coumarate-CoA ligase
CYP73A	Trans-cinnamate 4-monooxygenase
CMOT	Caffeic acid 3-O-methyltransferase
CYP84A	Ferulate-5-hydroxylase
CCR	Cinnamoyl-CoA reductase
HCT	Shikimate O-hydroxycinnamoyltransferase
CYP98A	5-O-(4-coumaroyl)-D-quinate 3′-monooxygenase
E2.1.1.104	Caffeoyl-CoA O-methyltransferase
K22395	Cinnamyl-alcohol dehydrogenase
PRDX6	Peroxiredoxin 6
UGT72E	Coniferyl-alcohol glucosyltransferase
E5.5.1.6	Chalcone isomerase
FLS	Flavonol synthase
CYP75B1	Flavonoid 3′-monooxygenase
DFR	Bifunctional dihydroflavonol 4-reductase
C12RT1	Flavanone 7-O-glucoside 2″-O-beta-L-rhamnosyltransferase
ANR	Anthocyanidin reductase
BZ1	Anthocyanidin 3-O-glucosyltransferase
3AT	Anthocyanidin 3-O-glucoside 6″-O-acyltransferase
GT1	Anthocyanidin 5,3-O-glucosyltransferase
FG3	Flavonol-3-O-glucoside/galactoside glucosyltransferase
AMOT	Flavonoid O-methyltransferase
C4H	Cinnamate-4-hydroxylase
COMT	Caffeic acid O-methyltransferase
DHZR	Dihydrozeatin riboside
cZR	cis-Zeatin riboside
tZR	trans-Zeatin riboside
IPR	Isopentenyl riboside
JA	Jasmonic acid
JA-ILE	Jasmonoyl-L-isoleucine
ABA	Abscisic acid
SA	Salicylic acid
SAR	Systemic acquired resistance
TRIT1	tRNA dimethylallyltransferase
IPT	Adenylate dimethylallyltransferase (cytokinin synthase)
CYP735A	Cytokinin trans-hydroxylase
UGT85A	UDP-glucosyltransferase 85 A
CKX	Cytokinin dehydrogenase
UGT76C1_2	Cytokinin-N-glucosyltransferase
AUX1	Auxin influx carrier
TIR1	Transport inhibitor response 1
IAA	Auxin-responsive protein IAA
ARF	Auxin response factor
GH3	Auxin responsive GH3 gene family
SAUR	SAUR family protein
AHK2_3_4	Arabidopsis histidine kinase 2/3/4
AHP	Histidine-containing phosphotransfer protein
ARR-A	Two-component response regulator ARR-A family
ARR-B	Two-component response regulator ARR-B family
GID1	Gibberellin receptor GID1
DELLA	DELLA protein
PIF3	Phytochrome-interacting factor 3
GID2	F-box protein GID2
PYL	Abscisic acid receptor PYR/PYL family
PP2C	Protein phosphatase 2 C
SNRK2	Serine/threonine-protein kinase SRK2
ABF	ABA responsive element binding factor
CTR1	Serine/threonine-protein kinase CTR1
ETR	Ethylene receptor
MKK4_5	Mitogen-activated protein kinase kinase 4/5
MPK6	Mitogen-activated protein kinase 6
EIN2	Ethylene-insensitive protein 2
EBF1_2	EIN3-binding F-box protein
EIN3	Ethylene-insensitive protein 3
ERF1	Ethylene-responsive transcription factor 1
BAK1	Brassinosteroid insensitive 1-associated receptor kinase 1
BKI1	BRI1 kinase inhibitor 1
BRI1	Protein brassinosteroid insensitive 1
BSK	BR-signaling kinase
TCH4	Xyloglucan: xyloglucosyl transferase TCH4
CYCD3	Cyclin D3
BIN2	Shaggy-related protein kinase (protein brassinosteroid insensitive 2)
BZR1_2	Brassinosteroid resistant 1/2
JAR1_4_6	Jasmonic acid-amino synthetase
COI-1	Coronatine-insensitive protein 1
JA	Jasmonate ZIM domain-containing protein
MYC2	Transcription factor MYC2
NPR1	Regulatory protein NPR1
TGA	Transcription factor TGA
PR1	Pathogenesis-related protein 1
GA	Gibberellic acid
BR	Brassinosteroid
ET	Ethylene
CTK	Cytokinin
ROS	Reactive oxygen species

Supplementary Information

The online version contains supplementary material available at https://doi.org/10.1186/s12870-026-08878-z.

Supplementary Material 1. Supplementary Table S1. Transcriptome data output statistics

Supplementary Material 2. Supplementary Table S2. Overview of the 1830 metabolites detected through extensively targeted metabolomics

Supplementary Material 3. Supplementary Table S3. Differentially significant metabolites for groups

Supplementary Material 4. Supplementary Table S4. Differentially significant metabolites enriched for groups

Supplementary Material 5. Supplementary Table S5. Type and content of phytohormones and their metabolites detected in this study

Supplementary Material 6. Supplementary Table S6. Five core co-expression modules bridging flavonoid metabolism and phytohormone signaling

Supplementary Material 7. Supplementary Fig. S1 Evaluation of the Panax ginseng plants and their apparent trait index. Supplementary Fig. S2 Transcriptome dynamic analysis. Supplementary Fig. S3 Top 20 pathways for differentially significant metabolites identified through extensively targeted metabolomics for KHQ vs ZYQ, JGQ vs KHQ, CSQ vs JGQ, CSQ vs CK, and CSQ vs LSD comparisons. Supplementary Fig. S4 Common KEGG-enriched pathways from the combined analysis of extensively targeted metabolomics and transcriptomics for KHQ vs ZYQ, JGQ vs KHQ, CSQ vs JGQ, CSQ vs CK, and CSQ vs LSD comparisons. Supplementary Fig. S5 Effect of Protopanaxadiol-type ginsenoside component stress on endogenous hormones in Panax ginseng plants. Supplementary Fig. S6 Common KEGG enrichment pathways for phytohormone-targeted metabolomics and transcriptomics data. Supplementary Fig. S7 The changes in key DEGs of the ko04075 pathway. Supplementary Fig. S8 Correlation analyses between physiological indices (MDA, SOD, POD, CAT, soluble protein, soluble sugar, proline) and molecular components of PPD-induced stress response. Supplementary Fig. S9 Module–trait correlation analysis of WGCNA co-expression modules with key metabolites and phytohormones in ginseng under protopanaxadiol-type ginsenosides stress

Acknowledgements
We would like to express our sincere gratitude to the Jilin Ginseng Academy for providing the research platform.

Authors' contributions
T.Z. analyzed and interpreted the data, conducted formal analysis, performed the investigation, developed methodology, created visualizations, managed software, and drafted the original manuscript. G.W. conducted investigation and curated data. X.L. conducted investigation and curated data. C.C. conceptualized the study, acquired funding, supervised the project, and managed project administration. X.H. conceptualized the study, validated results, and reviewed and edited the manuscript. All authors read and approved the final manuscript.

Funding
This study was funded by Jilin Provincial Key Research and Development Plan Project (20240305005YY) and Jilin Province Health Science and Technology Capacity Enhancement Project (2024A075).

Data availability
The raw RNA-seq data generated in this study have been deposited in the NCBI Sequence Read Archive (SRA) under BioProject accession number PRJNA1261682 (https://www.ncbi.nlm.nih.gov/bioproject/PRJNA1261682). The data are publicly available. All other data supporting the findings of this study are included in this article and its supplementary materials.

Declarations

Ethics approval and consent to participate
Not applicable. This study is not a clinical trial and animal testing.

Consent for publication
Not relevant.

Competing interests
The authors declare no competing interests.

Author details
[1]Jilin Ginseng Academy, Changchun University of Chinese Medicine, Changchun 130117, China
[2]School of Medical Technology, Beihua University, Jilin 132013, China

Received: 21 January 2026 / Accepted: 27 April 2026
Published online: 01 May 2026

References

1. Meng X, Zhang T, Chen C, Li Q, Liu J. Regulatory network of ginsenoside biosynthesis under Ro stress in the hairy roots of *Panax ginseng* revealed by RNA sequencing. Front Bioeng Biotechnol. 2022;101006386. https://doi.org/10.3389/fbioe.2022.1006386.
2. Yuan W, Wang QF, Pei WH, Li SY, Wang TM, Song HP, Teng D, Kang TG, Zhang H. Age-induced changes in ginsenoside accumulation and primary metabolic characteristics of *Panax Ginseng* in transplantation mode. J Ginseng Res. 2024;48(1):103–11. https://doi.org/10.1016/j.jgr.2023.09.003.
3. Sukweenadhi J, Balusamy SR, Kim YJ, Lee CH, Kim YJ, Koh SC, Yang DC. A growth-promoting bacteria, paenibacillus yonginensis DCY84T enhanced salt stress tolerance by activating defense-related systems in *Panax ginseng*. Front Plant Sci. 2018;9813. https://doi.org/10.3389/fpls.2018.00813.
4. Wang R, Zhou T, Wang Y, Dong J, Bai Y, Huang X, Chen C. Exploring the allelopathic autotoxicity mechanism of ginsenosides accumulation under ginseng decomposition based on integrated analysis of transcriptomics and metabolomics. Front Bioeng Biotechnol. 2024;121365229. https://doi.org/10.3389/fbioe.2024.1365229.
5. Xiang W, Chen J, Zhang F, Huang R, Li L. Autotoxicity in Panax notoginseng of root exudatesand their allelochemicals. Front Plant Sci. 2022;13:1020626. https://doi.org/10.3389/fpls.2022.1020626.
6. Liu C, Xia R, Tang M, Chen X, Zhong B, Liu X, Bian R, Yang L, Zheng J, Cheng K, et al. Improved ginseng production under continuous cropping through soil health reinforcement and rhizosphere microbial manipulation with biochar: a field study of *Panax ginseng* from Northeast China. Hortic Res. 2022;9:uhac108. https://doi.org/10.1093/hr/uhac108.
7. Zhang AH, Lei FJ, Fu JF, Zhou RJ, Zhang LX. Influence of exogenous ginsenosides on new forest soil microbial communities. Zhongguo Zhong Yao Za Zhi. 2017;42(24):4756–61. https://doi.org/10.19540/j.cnki.cjcmm.2017.0213.
8. Yang M, Zhang X, Xu Y, Mei X, Jiang B, Liao J, Yin Z, Zheng J, Zhao Z, Fan L, et al. Autotoxic ginsenosides in the rhizosphere contribute to the replant failure of Panax notoginseng. PLoS ONE. 2015;10(2):e0118555. https://doi.org/10.1371/journal.pone.0118555.
9. Liu J, Chen T, Zhang J, Li C, Xu Y, Zheng H, Zhou J, Zha L, Jiang C, Jin Y, et al. Ginsenosides regulate adventitious root formation in *Panax ginseng* via a CLE45-WOX11 regulatory module. J Exp Bot. 2020;71(20):6396–407. https://doi.org/10.1093/jxb/eraa375.
10. Shen Y, Fan M, Li G, Li Q, Meng X, Wang E, Chen C. Allelopathic effect of ginsenoside Rd on ginseng seeds and seedings. Appl Ecol Environ Res. 2023;21(1):59–72. https://doi.org/10.15666/aeer/2101_059072.
11. Li YL, Dai SY, Wang BY, Jiang YT, Ma YY, Pan LL, Wu K, Huang XQ, Zhang JB, Cai ZC, et al. Autotoxic Ginsenoside Disrupts Soil Fungal Microbiomes by Stimulating Potentially Pathogenic Microbes. Appl Environ Microbiol. 2020;86(9):e00130–20. https://doi.org/10.1128/AEM.00130-20.
12. Zhou T, Li Q, Huang X, Chen C. Analysis Transcriptome and Phytohormone Changes Associated with the Allelopathic Effects of Ginseng Hairy Roots Induced by Different-Polarity Ginsenoside Components. Molecules. 2024;29(8):1877. https://doi.org/10.3390/molecules29081877.
13. Pandita D, Pandita A, Wani SH, Abdelmohsen SAM, Alyousef HA, Abdelbacki AMM, Al-Yafrasi MA, Al-Mana FA, Elansary HO. Crosstalk of multi-Omics platforms with plants of therapeutic importance. Cells. 2021;10(6):1296. https://doi.org/10.3390/cells10061296.
14. Alami MM, Ouyang Z, Zhang Y, Shu S, Yang G, Mei Z, Wang X. The current developments in medicinal plant genomics enabled the diversification of secondary metabolites' biosynthesis. Int J Mol Sci. 2022;23(24):15932. https://doi.org/10.3390/ijms232415932.
15. Galindo-Prieto B, Eriksson L, Trygg J. Variable influence on projection (VIP) for OPLS models and its applicability in multivariate time series analysis. Chemometr Intell Lab Syst. 2015;146:297–304. https://doi.org/10.1016/j.chemolab.2015.05.001.
16. Vinaixa M, Samino S, Saez I, Duran J, Guinovart J, Yanes Ó. A Guideline to univariate statistical analysis for LC/MS-based untargeted metabolomics-derived data. Metabolites. 2012;2:775–95. https://doi.org/10.3390/metabo2040775.
17. Thévenot E, Roux A, Xu Y, Ezan E, Junot C. Analysis of the human adult urinary metabolome variations with age, body mass index, and gender by implementing a comprehensive workflow for univariate and OPLS statistical analyses. J Proteome Res. 2015;14 8:3322–35. https://doi.org/10.1021/acs.jproteome.5b00354.
18. Langfelder P, Horvath S. WGCNA: an R package for weighted correlation network analysis. BMC Bioinformatics. 2008;9:559–559. https://doi.org/10.1186/1471-2105-9-559.
19. Bajguz A, Piotrowska-Niczyporuk A. Biosynthetic pathways of hormones in plants. Metabolites. 2023;13(8):884. https://doi.org/10.3390/metabo13080884.
20. Pan LY, Zhou J, Sun Y, Qiao BX, Wan T, Guo RQ, Zhang J, Shan DQ, Cai YL. Comparative transcriptome and metabolome analyses of cherry leaves spot disease caused by Alternaria alternata. Front Plant Sci. 2023;141129515. https://doi.org/10.3389/fpls.2023.1129515.
21. Meng X, Huang X, Li Q, Wang E, Chen C. Application of UPLC-Orbitrap-HRMS targeted metabolomics in screening of allelochemicals and model plants of ginseng. J Plant Physiol. 2023:285:153996. https://doi.org/10.1016/j.jplph.2023.153996
22. Miao Y, Li H, Pan J, Zhou B, He T, Wu Y, Zhou D, He W, Chen L. Salicylic acid modulates secondary metabolism and enhanced colchicine accumulation in long yellow daylily (Hemerocallis citrina). AoB Plants. 2024;16(4):plae029. https://doi.org/10.1093/aobpla/plae029.
23. Wang X, Zhao W, Wei X, Song S, Dong S. The application potential of mepiquat chloride in soybean: improvement of yield characteristics and drought resistance. BMC Plant Biol. 2024;24(1):310. https://doi.org/10.1186/s12870-024-05028-1.
24. Legendre L, Rueter S, Heinstein PF, Low PS. Characterization of the oligogalacturonide-induced oxidative burst in cultured soybean (Glycine max) cells. Plant Physiol. 1993;102(1):233–40. https://doi.org/10.1104/pp.102.1.233.
25. Szechyńska-Hebda M, Ghalami RZ, Kamran M, Van Breusegem F, Karpiński S. To be or not to be? Are reactive oxygen species, antioxidants, and stress

signalling universal determinants of life or death? Cells. 2022;11(24):4105. https://doi.org/10.3390/cells11244105.
26. Das K, Roychoudhury A. Reactive oxygen species (ROS) and response of antioxidants as ROS-scavengers during environmental stress in plants. Front Environ Sci. 2014;2(53). https://doi.org/10.3389/fenvs.2014.00053.
27. Kaplan F, Kopka J, Sung DY, Zhao W, Popp M, Porat R, Guy CL. Transcript and metabolite profiling during cold acclimation of Arabidopsis reveals an intricate relationship of cold-regulated gene expression with modifications in metabolite content. Plant J. 2007;50(6):967–81. https://doi.org/10.1111/j.1365-313X.2007.03100.x.
28. Hayat S, Hayat Q, Alyemeni MN, Wani AS, Pichtel J, Ahmad A. Role of proline under changing environments: a review. Plant Signal Behav. 2012;7(11):1456–66. https://doi.org/10.4161/psb.21949.
29. Yang L, Yang Q, Zhang L, Ren F, Zhang Z, Jia Q. Integrated Metabolomics and Transcriptomics Analysis of Flavonoid Biosynthesis Pathway in Polygonatum cyrtonema Hua. Molecules. 2024;29(10):2248. https://doi.org/10.3390/molecules29102248.
30. Sun C, Deng L, Du M, Zhao J, Chen Q, Huang T, Jiang H, Li CB, Li C. A transcriptional network promotes anthocyanin biosynthesis in Tomato flesh. Mol Plant Mol Plant. 2020;13(1):42–58. https://doi.org/10.1016/j.molp.2019.10.010.
31. Li Z, Ahammed GJ. Hormonal regulation of anthocyanin biosynthesis for improved stress tolerance in plants. Plant Physiol Biochem. 2023;201:107835. https://doi.org/10.1016/j.plaphy.2023.107835.
32. Sunil L, Shetty NP. Biosynthesis and regulation of anthocyanin pathway genes. Appl Microbiol Biotechnol. 2022;106(5–6):1783–98. https://doi.org/10.1007/s00253-022-11835-z.
33. Li P, Li YJ, Zhang FJ, Zhang GZ, Jiang XY, Yu HM, Hou BK. The Arabidopsis UDP-glycosyltransferases UGT79B2 and UGT79B3, contribute to cold, salt and drought stress tolerance via modulating anthocyanin accumulation. Plant J. 2017;89(1):85–103. https://doi.org/10.1111/tpj.13324.
34. Vogt T. Phenylpropanoid biosynthesis. Mol Plant. 2010;3(1):2–20. https://doi.org/10.1093/mp/ssp106.
35. Glagoleva AY, Vikhorev AV, Shmakov NA, Morozov SV, Chernyak EI, Vasiliev GV, Shatskaya NV, Khlestkina EK, Shoeva OY. Features of activity of the phenylpropanoid biosynthesis pathway in melanin-accumulating barley grains. Front Plant Sci. 2022;13923717. https://doi.org/10.3389/fpls.2022.923717.
36. Dong NQ, Lin HX. Contribution of phenylpropanoid metabolism to plant development and plant–environment interactions. J Integr Plant Biol. 2021;63(1):180–209. https://doi.org/10.1111/jipb.13054.
37. Zhu C, Zhang S, Fu H, Zhou C, Chen L, Li X, Lin Y, Lai Z, Guo Y. Transcriptome and phytochemical analyses provide new insights into long non-coding RNAs modulating characteristic secondary metabolites of oolong tea (Camellia sinensis) in solar-withering. Front Plant Sci. 2019;101638. https://doi.org/10.3389/fpls.2019.01638.
38. Chung IM, Lim JJ, Ahn MS, Jeong HN, An TJ, Kim SH. Comparative phenolic compound profiles and antioxidative activity of the fruit, leaves, and roots of korean ginseng (*Panax ginseng* Meyer) according to cultivation years. J Ginseng Res. 2016;40(1):68–75. https://doi.org/10.1016/j.jgr.2015.05.006.
39. Sun G, Wang J, Xu X, et al Panax ginseng Meyer cv. Silvatica phenolic acids protect DNA from oxidative damage by activating Nrf2 to protect HFF-1 cells from UVA-induced photoaging. J Ethnopharmacol. 2023;302(Pt A):115883. . https://doi.org/10.1016/j.jep.2022.115883.
40. Pourcel L, Routaboul JM, Cheynier V, Lepiniec L, Debeaujon I. Flavonoid oxidation in plants: from biochemical properties to physiological functions. Trends Plant Sci. 2007;12(1):29–36. https://doi.org/10.1016/j.tplants.2006.11.006.
41. Zhuang WB, Li YH, Shu XC, Pu YT, Wang XJ, Wang T, Wang Z. The classification, molecular structure and biological biosynthesis of flavonoids, and their roles in biotic and abiotic stresses. Molecules. 2023;28(8):3599. https://doi.org/10.3390/molecules28083599.
42. Liu W, Feng Y, Yu S, Fan Z, Li X, Li J, Yin H The Flavonoid biosynthesis network in plants. Int J Mol Sci. 2021;22(23):12824. . https://doi.org/10.3390/ijms222312824.
43. Yuan Y, Zuo J, Zhang H, Zu M, Liu S. Analysis of the different growth years accumulation of flavonoids in Dendrobium moniliforme (L.) Sw. by the integration of metabolomic and transcriptomic approaches. Front Nutr. 2022;9928074. https://doi.org/10.3389/fnut.2022.928074.
44. Song Y, Hanner RH, Meng B. Transcriptomic Analyses of grapevine leafroll-associated virus 3 infection in leaves and berries of 'Cabernet Franc'. Viruses. 2022;14(8):1831. https://doi.org/10.3390/v14081831.
45. Li GL, Tang ZS, Song ZG, Shi XB, Liu CL, Chen Q, Liu HB. Integrated transcriptomic and metabolomic analysis reveal the molecular and metabolic basis of flavonoids in Chinese sour jujube fruits in different harvest times. Postharvest Biol Technol. 2023;209112685. https://doi.org/10.1016/j.postharvbio.2023.112685.
46. Cabello-Hurtado F, El Amrani A. Phenanthrene-Induced cytochrome P450 genes and phenanthrene tolerance associated with arabidopsis thaliana CYP75B1 gene. Plants (Basel). 2024;13(12):1692. https://doi.org/10.3390/plants13121692.
47. Wang Y, Zhou LJ, Wang Y, Liu S, Geng Z, Song A, Jiang J, Chen S, Chen F. Functional identification of a flavone synthase and a flavonol synthase genes affecting flower color formation in Chrysanthemum morifolium. Plant Physiol Biochem. 2021;166:1109–20. https://doi.org/10.1016/j.plaphy.2021.07.019.
48. Ye H, Luo J, Hu D, Yang S, Zhang A, Qiu Y, Ma X, Wang J, Hou J, Bai J. Total flavonoids of crocus sativus petals release tert-Butyl hydroperoxide-induced oxidative stress in BRL-3A cells. Oxid Med Cell Longev. 2021;20215453047. https://doi.org/10.1155/2021/5453047.
49. Kojima M, Makita N, Miyata K, Yoshino M, Iwase A, Ohashi M, Surjana A, Kudo T, Takeda-Kamiya N, Toyooka K, et al. A cell wall-localized cytokinin/purine riboside nucleosidase is involved in apoplastic cytokinin metabolism in Oryza sativa. Proc Natl Acad Sci U S A. 2023;36120. https://doi.org/10.1073/pnas.2217708120.
50. Li SM, Zheng HX, Zhang XS, Sui N. Cytokinins as central regulators during plant growth and stress response. Plant Cell Rep. 2021;40(2):271–82. https://doi.org/10.1007/s00299-020-02612-1.
51. Durán-Medina Y, Díaz-Ramírez D, Marsch-Martínez N. Cytokinins on the Move. Front Plant Sci. 2017;8:146. https://doi.org/10.3389/fpls.2017.00146.
52. Zaheer MS, Ali HH, Erinle KO, Wani SH, Okon OG, Nadeem MA, Nawaz M, Bodlah MA, Waqas MM, Iqbal J, et al. Inoculation of Azospirillum brasilense and exogenous application of trans-zeatin riboside alleviates arsenic induced physiological damages in wheat (Triticum aestivum). Environ Sci Pollut Res Int. 2022;29(23):33909–19. https://doi.org/10.1007/s11356-021-18106-w.
53. Jameson PE, Zeatin. The 60th anniversary of its identification. Plant Physiol. 2023;192(1):34–55. https://doi.org/10.1093/plphys/kiad094.
54. Verma V, Ravindran P, Kumar PP. Plant hormone-mediated regulation of stress responses. BMC Plant Biol. 2016;16:86. https://doi.org/10.1186/s12870-016-0771-y.
55. Zhao S, Li M, Ren X, Wang C, Sun X, Sun M, Yu X, Wang X. Enhancement of broad-spectrum disease resistance in wheat through key genes involved in systemic acquired resistance. Front Plant Sci. 2024;151355178. https://doi.org/10.3389/fpls.2024.1355178.
56. Li C, Xia Y, Xiang F, Cao S, Zhou M, Wang K, Zou Y, Li M, Zheng Y. β-Aminobutyric acid activates SA-signalling systemic acquired resistance in peach fruit by suppressing the circadian clock associated protein1. Int J Biol Macromol. 2025;300140040. https://doi.org/10.1016/j.ijbiomac.2025.140040.
57. Yang J, Duan G, Li C, et al. The Crosstalks Between Jasmonic Acid and Other Plant Hormone Signaling Highlight the Involvement of Jasmonic Acid as a Core Component in Plant Response to Biotic and Abiotic Stresses. Front Plant Sci. 2019;10. https://doi.org/10.3389/fpls.2019.01349.
58. Aerts N, Mendes MP, Van Wees SCM. Multiple levels of crosstalk in hormone networks regulating plant defense. Plant J. 2020;105:489–504. https://doi.org/10.1111/tpj.15124.
59. Van Der Does D, Leon-Reyes A, Koornneef A, et al. Salicylic Acid Suppresses Jasmonic Acid Signaling Downstream of SCFCOI1-JAZ by Targeting GCC Promoter Motifs via Transcription Factor ORA59[C][W][OA]. Plant Cell. 2013;25:744–61. https://doi.org/10.1105/tpc.112.108548.
60. Verma V, Ravindran P, Kumar PP. Plant hormone-mediated regulation of stress responses. BMC Plant Biol. 2016;16. https://doi.org/10.1186/s12870-016-0771-y.
61. Huang X, Hou L, Meng J, et al. The Antagonistic Action of Abscisic Acid and Cytokinin Signaling Mediates Drought Stress Response in Arabidopsis. Mol Plant. 2018;11(7):970–82. https://doi.org/10.1016/j.molp.2018.05.001.

Publisher's note